Hindawi
Geofluids
Volume 2024, Article ID 8071443, 11 pages
https://doi.org/10.1155/2024/8071443

Research Article

Impact of Tool Eccentricity on Acoustic Logging Response in Horizontal Wells: Insights from Physical Simulation Experiments

Yuanjun Zhang,[1,2] Dong Wu,[3] Maojie Liao,[4] Xuewen Shi,[4] Feng Chen,[1,2] Chengguang Zhang,[1,2] Ming Cai,[1,2] and Jun Tang[1,2]

[1]*Key Laboratory of Exploration Technologies for Oil and Gas Resources (Yangtze University), Ministry of Education, Wuhan 430100, China*
[2]*College of Geophysics and Petroleum Resources, Yangtze University, Wuhan 430100, China*
[3]*Information Center, Engineering Technology R&D Company Limited, CNPC, Beijing 102206, China*
[4]*Shale Gas Institute of PetroChina Southwest Oil & Gas Field Company, Chengdu 610051, China*

Correspondence should be addressed to Ming Cai; caiming@yangtzeu.edu.cn

Received 19 September 2023; Revised 14 December 2023; Accepted 15 December 2023; Published 5 January 2024

Academic Editor: Tianshou Ma

Horizontal wells are extensively utilized in the development of unconventional reservoirs. However, the logging responses and formation evaluation in horizontal wells can be impacted by factors like anisotropy and tool eccentricity. To investigate the influence of tool eccentricity on acoustic logging response, physical simulation experiments of array acoustic logging were conducted in a scaled borehole formation model under different tool eccentricity conditions. The experimental data were analyzed, and the findings revealed that when the receiver array is parallel to the borehole axis, the P-wave slowness and S-wave slowness remain unaffected by tool eccentricity. However, the amplitudes of the P-wave and S-wave decrease significantly with increasing tool eccentricity, following an approximate negative exponential pattern. Additionally, when the transmitter is centered and the receiver array intersects the borehole axis at an angle, the wave velocities increase significantly with tool eccentricity, with the P-wave velocity showing a faster increase. Conversely, when the transmitter is eccentric and the receiver array intersects the borehole axis at an angle, the wave velocity decreases notably with tool eccentricity, and the P-wave velocity decreases even faster. These findings contribute to a better understanding of the impact of tool eccentricity on array acoustic logging response in horizontal wells and offer guidance for developing correction schemes to address this effect.

1. Introduction

Over recent decades, the oil industry has seen a significant evolution in drilling technologies, especially in the application of horizontal wells. These methodologies have not only fostered the emergence of new oilfields but have also redefined strategies for optimizing existing ones. Horizontal wells provide distinctive advantages for various reservoirs such as fractured, both thin and thick formations, reservoirs requiring artificial water injection, and low-permeability types like shale gas, coalbed methane, tight gas, and offshore deposits [1–21]. The primary benefits of horizontal wells are as follows [1, 4, 19–21]: (1) enhanced production from fractured formations (the casing of horizontal wells can penetrate natural fracture zones, significantly increasing oil and gas output in fractured formations), (2) improved output from low porosity and low-permeability reservoirs (horizontal wells increase the contact area between the borehole and the formation, enabling passage through reservoirs with better permeability, thereby enhancing oil and gas production from such low porosity and low-permeability reservoirs), (3) efficient oil and gas recovery (horizontal wells allow for directional drilling based on the distribution of oil, gas, and water, helping to control water and gas cones and consequently increasing oil and gas output), and (4) cost-effective and efficient exploration and development (horizontal wells significantly reduce drilling density, resulting in cost savings in exploration and development and increased overall efficiency).

Acoustic logging plays a crucial role in evaluating reservoirs, fractures, and anisotropy. However, the existing methods for processing and interpreting acoustic logging data from horizontal wells are incomplete and unsophisticated. Many of these methods are directly adapted from vertical wells, despite significant differences between horizontal wells and vertical wells. As a result, there is an inconsistency between the processing and interpretation results of acoustic logging data from horizontal wells and the actual conditions. Several primary factors influence acoustic logging in horizontal wells [2, 7–9, 21–25]. (1) Formation anisotropy: the borehole of a horizontal well may intersect the formation interface at an angle, resulting in nonrotational symmetry around the borehole. This leads to a different propagation process of mode waves compared to straight wells. (2) Borehole shape: gravity causes the lower part of the borehole to be pulled into a groove by the drill pipe, resulting in a key-shaped borehole. Rock chips that are not circulated out of the well are deposited in these grooves, affecting the propagation of sound waves. (3) Mud fluid invasion: in horizontal wells, there is a pressure difference between the formation and the borehole, leading to mud fluid intrusion into the formation. The shape of the invaded mud is generally asymmetric, often taking the form of "teardrops" and "ellipses." (4) Tool eccentricity: due to the influence of gravity, logging tools face challenges in centering within the borehole, which significantly impacts the acoustic logging response. In summary, addressing these factors is essential to improve the accuracy and effectiveness of acoustic logging data interpretation in horizontal wells.

In summary, these complexities necessitate a more tailored approach to processing and interpreting acoustic logging data from horizontal wells. Addressing these specific factors will greatly enhance the accuracy and effectiveness of acoustic logging, further improving the precision and reliability of reservoir evaluation in horizontal wells.

Numerous scholars have extensively researched the impact of acoustic logging responses on horizontal wells. Cong and Qiao [26] conducted simulations on the acoustic logging response of horizontal wells passing through the formation interface. Wang et al. [12, 27] employed the finite element method to simulate the distribution and variation of the acoustic field generated by multipole acoustic logging while drilling in horizontal and high-angle deviated wells. The results indicated that certain wave modes observed in the monopole measurement method may also appear in the dipole measurement method when the instrument is eccentric. Moreover, the intensity of the drill collar bending wave significantly increases with tool eccentricity. Huang and Torres-Verdín [19] reported a poor correlation of array waveforms measured by array acoustic logging in deviated and horizontal wells, rendering the traditional slowness extraction method based on waveform correlation unsuitable. Instead, they used the head wave arrival time to calculate P-wave and S-wave slowness. Additionally, Huang and Torres-Verdín proposed a method for simulating the propagation time of the first P-wave in horizontal wells using a one-dimensional numerical simulation method. The difference between the P-wave slowness curve simulated by this method and the slowness curve obtained by three-dimensional finite difference simulation was within 5%, saving 99% of CPU computation time. Wang and Herrera [20] utilized a three-dimensional finite difference time-domain method to simulate acoustic wave propagation in deviated and horizontal wells, analyzing the impact of formation interfaces on P-wave, S-wave, and bending wave propagation. However, they did not investigate the effects of borehole shape, tool eccentricity, and mud invasion on the propagation of acoustic waves in horizontal wells. Su and Cai [28] employed the three-dimensional finite difference method to simulate the full waveforms of array acoustic logging under borehole enlargement conditions in horizontal wells, studying the impact of borehole enlargement on acoustic logging response.

The above results primarily pertain to the numerical simulation study of the influence of interface near-borehole, tool eccentricity, and borehole conditions on acoustic logging response in horizontal wells. Currently, there is a lack of quantitative research on the effect of tool eccentricity on array acoustic logging response in horizontal wells. Enhancing the accuracy of acoustic logging data processing and interpretation in horizontal wells holds crucial importance for oilfield development, output, and numerical simulation research of acoustic logging responses. Consequently, it is essential to conduct in-depth investigations into the impact of various geological conditions and measurement environments on acoustic logging response in horizontal wells.

In this investigation, we systematically probe the influence of tool eccentricity on the response of array acoustic logging, underpinned by meticulous physical simulation experiments. Central to this research is the endeavor to refine the distortions induced by tool eccentricity during acoustic logging in horizontal wells. Furthermore, a primary objective is to integrate these empirical insights into improved interpretation methodologies for horizontal well logging. This present study diverges from antecedent investigations in two principal dimensions: On the one hand, physical simulation experiments were conducted to elucidate the effects of tool eccentricity on array acoustic logging in horizontal wells. On the other hand, we undertook a detailed quantitative analysis to understand how tool eccentricity affects the velocities and amplitudes of both P-waves and S-waves in horizontal wells, leading to the development of correlational charts. The subsequent sections of this manuscript are systematically organized. The next section details the underlying principles and methods that inform the physical simulation experiments for array acoustic logging. Following this, an extensive overview of the experiments conducted across varied eccentricity conditions is provided. Once the data has been compiled, emphasis is placed on the extraction and analysis of the velocities and amplitudes of P-waves and S-waves. An in-depth discussion follows, examining the relationships between these measurements and their respective eccentricity states. The manuscript concludes by summarizing the primary findings and drawing conclusions based on the research results.

2. Experimental Method for Acoustic Logging Simulation in Horizontal Wells

2.1. Experimental Equipment. The experimental equipment consists of an ultrasonic pulse signal generation and reception instrument (CTS-8077PR), a digital oscilloscope (UTC2102CEL), a dynamic test analyzer (TST3206), an acoustic tool, and a scaled borehole formation model. The complete physical simulation experiment system is shown in Figure 1. Figure 2 illustrates the self-developed single-transmitter single-receiver acoustic tool, and the tool is used for equivalent array acoustic logging physical simulation experiment. Array acoustic full waveforms can be acquired by measuring multiple times with different transmitter-receiver spacings. Additionally, different states of tool eccentricity can be achieved by installing acoustic transducers at various holes in the clamping unit (Figure 2(b)). The formation model with a scaled borehole is made of dense limestone. The formation model is a cuboid with dimensions of $100\,\text{cm} \times 50\,\text{cm} \times 50\,\text{cm}$, and the diameter of the borehole is 4 cm. The density of the model is $2699\,\text{kg/m}^3$, and the P-wave and S-wave velocities of the model are 5800 m/s and 3000 m/s, respectively.

2.2. Experimental Principle. Figure 1(a) depicts the formation model with a scaled borehole, constructed using standard limestone rocks. The experimental acoustic tool is positioned in the borehole. Both ends of the acoustic tool are connected to CTS-8077PR, which applies excitation signals to the transmitter, causing it to emit acoustic signals. These acoustic signals propagate through the fluid in the borehole and the surrounding media. Eventually, the receiver captures the acoustic signals, and the results are displayed on the oscilloscope. Simultaneously, the waveform signals are subjected to digital processing using a high-precision signal acquisition instrument, and the full waveform data are recorded. Additionally, multiple sets of full waveforms can be produced by changing the distance between the transmitter and receiver. Then, these full waveforms are classified and combined to derive array wave signals received by a single transmitter and multiple receivers, enabling the realization of array acoustic logging simulation measurement.

As shown in Figure 2, the acoustic tool includes a transmitting transducer, a receiving transducer, and a transducer clamping unit. The tool is connected to a high-precision traction system, and then, the position of the tool can be controlled precisely in the scaled borehole model. Adjusting the positions of the transducers in the clamping unit produces variations in tool eccentricity states, and the corresponding experiments are conducted. Finally, the experimental full waveform data are analyzed, and the effect of tool eccentricity on acoustic logging responses is revealed.

2.3. Experimental Measurement Method. To comprehensively analyze the impact of tool eccentricity on the acoustic logging response in horizontal wells, the eccentricity states are categorized as follows: the receiver array is parallel to the borehole axis, and the receiver array intersects the borehole axis at an angle. The latter is further subdivided into two cases: the transmitter axis coincides with the borehole axis, and the transmitter axis deviates from the borehole axis. Figure 3 illustrates the eccentricity states of the receiver arrays parallel to the borehole axis, while Figures 4 and 5 show two eccentricity states: (1) the transmitter axis coincides with the borehole axis and the receiver arrays intersect the borehole axis at an angle, and (2) the transmitter axis deviates from the borehole axis and the receiver arrays intersect the borehole axis at an angle. The red dot represents the transmitter, the blue dots denote the receivers, and the red dotted lines illustrate the propagation path of the mode wave.

The specific experimental measurements proceed as follows:

(1) The scaled borehole model was lifted and placed in the water tank, and the tank was filled with water

(2) The eccentricity state of the acoustic tool was set, and an appropriate spacing between the transmitter and receiver (TR spacing) was adjusted. Note that the TR spacing refers to the distance between adjacent receiver centers. The physical simulation experimental system for equivalent array acoustic logging (shown in Figure 1) was connected, and a bubble removal device was used to eliminate bubbles in the borehole

(3) The acoustic tool was precisely positioned using the high-precision tool traction device. In the experiment, the acoustic tool moved through the scaled borehole at a set interval. At each designated position, the acoustic excitation system triggered the transmitting transducer to emit signals, which were then immediately received and recorded by the receiving transducer and acquisition system. After each measurement, we obtained full waveforms corresponding to various positions

(4) After the TR spacing of the acoustic tool was adjusted, we repeated step 3 and obtained full waveforms for various positions at different TR spacing conditions

(5) The full waveforms recorded at the same position with different TR spacings were combined, and an equivalent array full waveform set was obtained

(6) Finally, the eccentricity state of the acoustic tool was altered, and the above measurement processes were conducted again, and then, array full waveform sets were obtained at different eccentricity states

3. Experimental Measurement and Analysis of Physical Simulation of Array Acoustic Logging under Eccentric Conditions

3.1. Experimental Measurement and Analysis of Receiving Transducer Array Parallel to the Borehole Axis

3.1.1. Experimental Measurement and Data Processing. Following the described experimental method, physical simulation measurements of array acoustic logging were

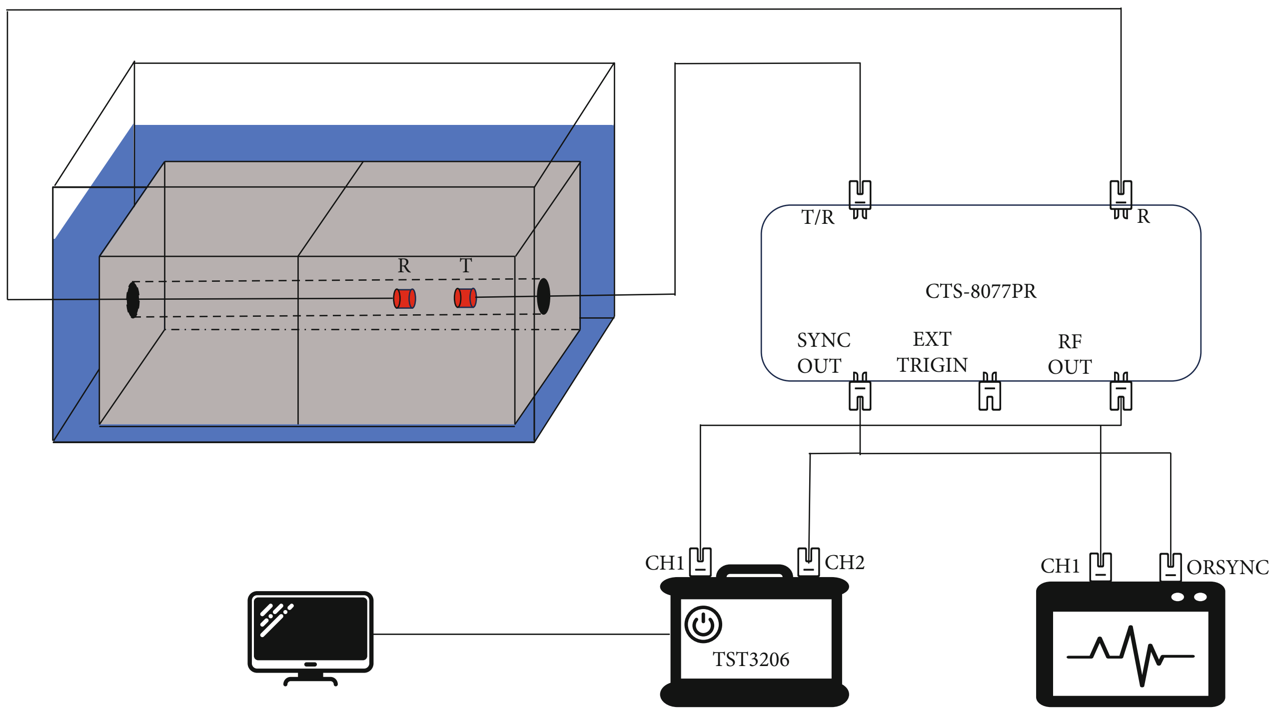

(a)

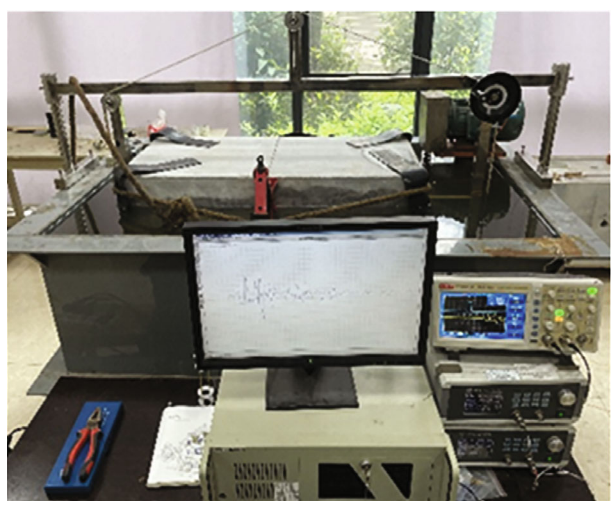

(b)

Figure 1: Experimental measurement system for physical simulation of array acoustic logging, where (a) is a schematic diagram and (b) is a photograph of the system.

conducted with the receiver array axis parallel to the borehole axis. As depicted in Figure 6, the P-wave and S-wave features are distinct, exhibiting a high signal-to-noise ratio. The STC (slowness-time coherence) method [26, 27] was applied to extract the wave mode slowness from the array waveforms shown in Figure 6. The slowness-time coherence plot is presented in Figure 7. According to the STC processing results, the wave velocities for P-wave and S-wave were quantified as 5839.4 m/s and 2944.8 m/s, respectively. The values obtained closely aligned with the actual P-wave and S-wave velocities of the borehole model, thereby confirming the feasibility of the horizontal well acoustic logging physical simulation system and its measurement approach.

Through the application of the STC method, array full waveforms from various eccentricity states were analyzed, and velocities of P-wave and S-wave were determined. Based on these velocities, arrival times of the head wave were subsequently estimated. P-wave and S-wave amplitudes were determined by assessing the peak and trough differences within the first or two periods following the onset of each wave. To simplify the calculation process, this experiment opted for computing a single waveform to determine amplitude. A comprehensive summary of these results can be found in Table 1.

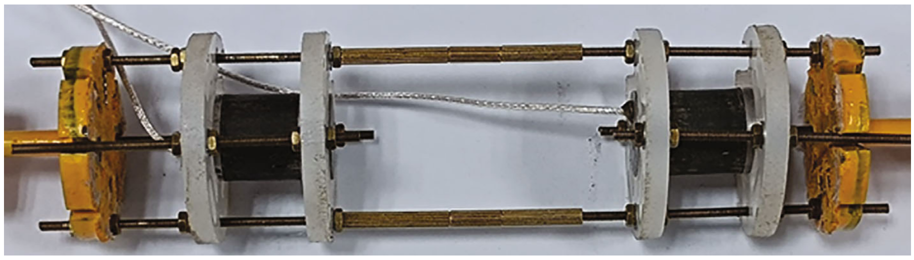

(a)

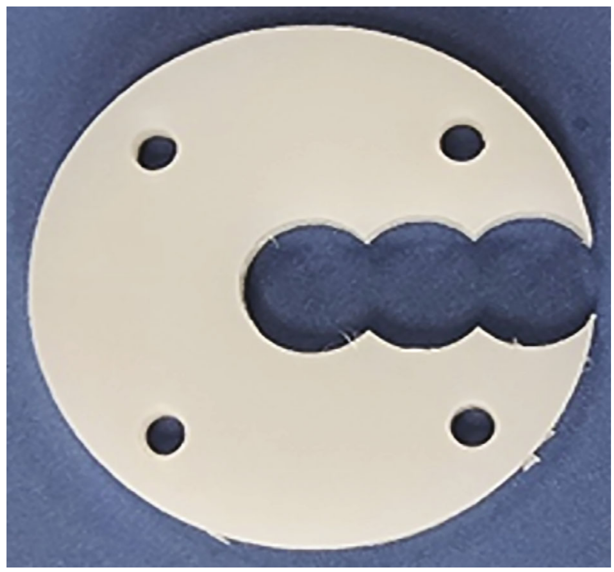

(b)

FIGURE 2: Physical diagram of the self-developed single-transmitter single-receiver acoustic tool where (a) showcases an actual photograph and (b) depicts the acoustic transducer clamping unit.

3.1.2. Analysis of the Effect of Tool Eccentricity on Mode Waves. Further analysis was conducted to understand the impact of tool eccentricity states on characteristic parameters, such as wave velocities in array acoustic logging. The variations of P-wave and S-wave velocities with the eccentric state when the receiver array axis is parallel to the borehole axis are detailed in Table 1. Figure 8, constructed using data from Table 1, illustrates that no significant variations in P-wave and S-wave velocities occurred with changes in eccentric states when the receiver array axis was parallel to the borehole axis. This observation is easily explained by considering the propagation path of waves.

To delve deeper into the influence of tool eccentricity on acoustic logging amplitude, eccentricity states were bifurcated into two primary categories. The first comprised cases where the receiver array axis coincided with the transmitter axis, and both were parallel to the borehole axis, including eccentricity states (0), (1), and (2). Here, the separation between the acoustic system axis and the borehole axis is denoted as eccentricity distance "a." The second category encompassed the centered state (0) alongside other eccentricity conditions (states 3 to 8), with the distance between the transmitter axis and receiver array axis referred to as eccentric distance "b." Variations in P-wave and S-wave amplitudes concerning eccentric distances "a" and "b" when the receiver array remains parallel to the borehole axis, derived from the analysis in Table 1, are depicted in Figure 9. Specifically, Figures 9(a) and 9(b) illustrate how the amplitudes of P-wave and S-wave vary with eccentricity distance "a." In contrast, Figures 9(c) and 9(d) show how the amplitudes of P-wave and S-wave vary with eccentricity distance "b." It was observed that amplitudes for both P-wave and S-wave declined exponentially with increasing eccentricity distances "a" and "b."

3.2. Experimental Measurement and Analysis of the Receiver Array Intersect the Borehole Axis at an Angle. In scenarios where the transmitter coincided with the borehole axis and the receiver array intersected the borehole axis at an angle, three states were studied with angles of 7.75°, 11.54°, and 22.21° between the receiver array and the borehole axis. Conversely, when the transmitter deviated from the borehole axis, five angles were investigated: 7.75°, 11.54°, 15.23°, 22.21°, and 39.24°. Figure 10 presents the array waveforms for the case the transmitter coincided with the borehole axis and the receiver array intersected the borehole axis at 22.21°. The STC method was employed to process the array waveforms for the cases where the transmitter coincided with the borehole axis and the receiver array intersected the borehole axis at an angle. Both the P-wave and S-wave velocities

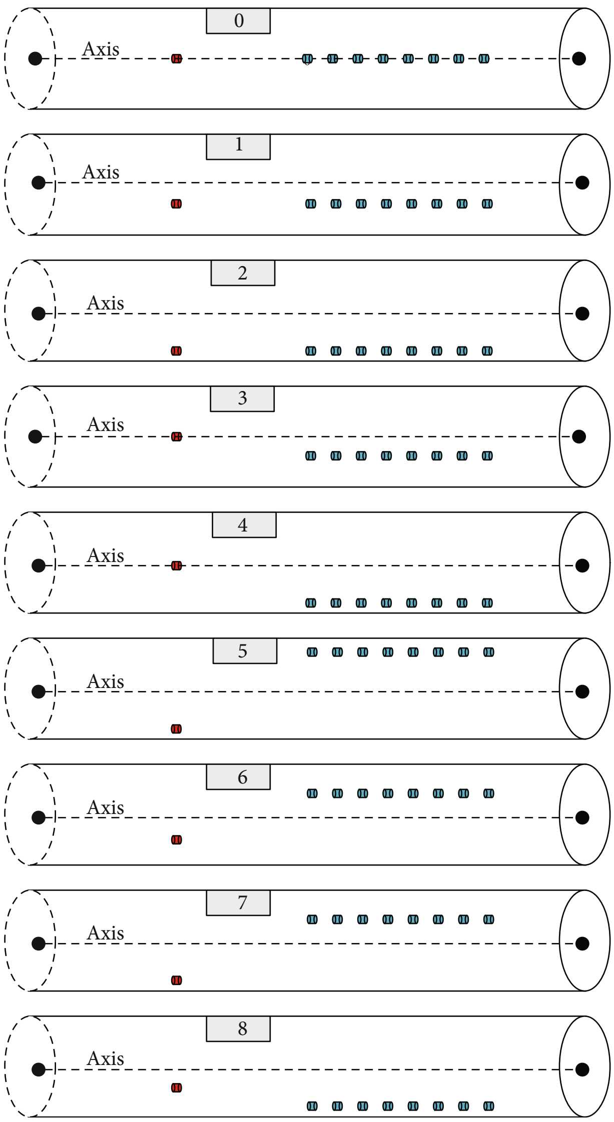

FIGURE 3: The eccentricity states where both the receiver array axis and the transmitter axis are parallel to the borehole axis.

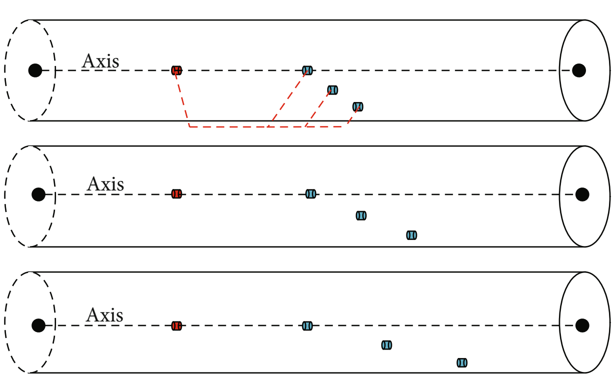

FIGURE 4: The transmitter axis coincides with the borehole axis, and the receiver arrays intersect the borehole axis at an angle.

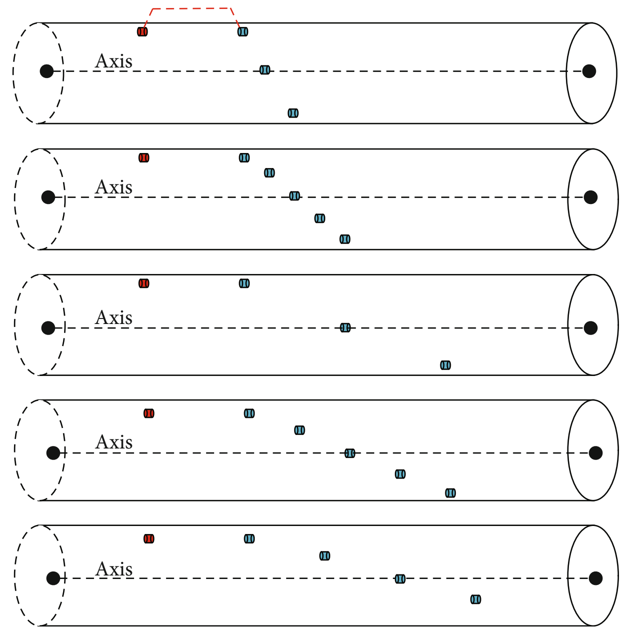

FIGURE 5: The transmitter axis deviates from the borehole axis, and the receiver arrays intersect the borehole axis at an angle.

were extracted, and the velocities of both P-waves and S-waves are determined and tabulated in Table 2. Figure 11 graphically represents the relationship between these velocities and the eccentricity angle of the receiver array, derived from Table 2 data. As discerned from the figure, when the transmitter coincided with the borehole axis and the receiver array intersected the borehole axis at an angle, the P-wave and S-wave velocities were significantly higher than those measured when the tool is in a noneccentric position. Furthermore, with an increase in the angle of the eccentricity of the receiver array, both P-wave and S-wave velocities exhibit a nearly linear increase, with the P-wave velocities ascending more rapidly. The observed phenomenon mainly arises from varying propagation path lengths within the borehole fluid for sliding waves reaching different receivers, analyzed as follows: as depicted in Figure 4, red denotes the transmitter, and blue indicates the receivers (labeled as receiver 1, receiver 2, and receiver 3 from left to right). According to Fermat's principle, acoustic waves tend to propagate through the shortest path. Distances traveled to receiver 1 (L1) and receiver 2 (L2) differ as illustrated. Compared to the centered position, L2 notably shortens, advancing the arrival time at receiver 2 under a constant travel time to receiver 1. Consequently, this reduces the time difference within the receiver array while maintaining a constant calculated distance, leading to an increased calculated velocity.

In instances where the transmitter axis deviates from the borehole axis and the receiver array axis intersects the borehole axis at an angle, the STC method was utilized to extract the head wave correlation coefficient across varying eccentric angles, subsequently determining P-wave and S-wave velocities. These findings are compiled in Table 3. The data from Table 3 illustrates the relationships of both P-wave and S-wave velocities with the eccentricity angle, as shown

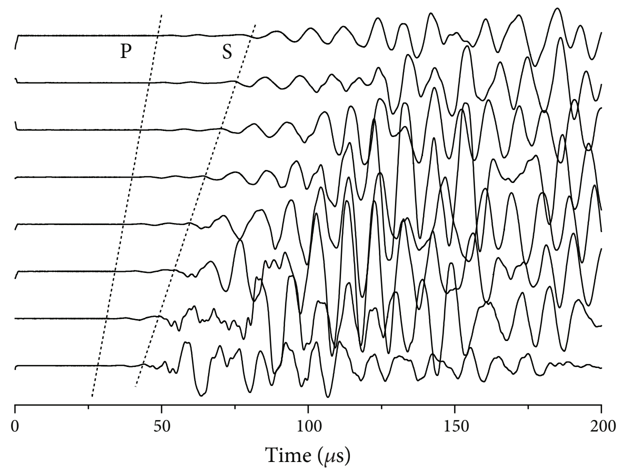

FIGURE 6: Array full waveforms when the tool is in the center of the borehole.

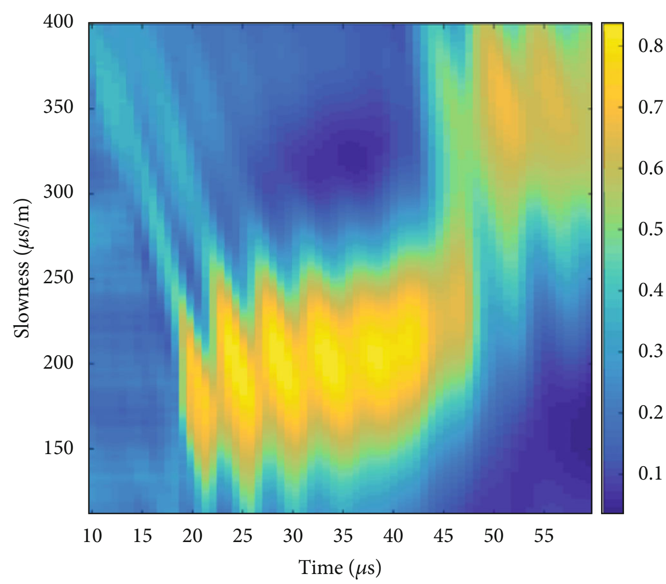

FIGURE 7: Slowness-time coherence plot for array full waveforms when the tool is in the center of the borehole.

TABLE 1: Statistical table of P-wave and S-wave velocities and amplitudes in different eccentric states when the receiver array is parallel to the borehole axis, where V_p represents the P-wave velocities and V_s represents the velocities of the S-wave.

Eccentricity states	V_p (m/s)	V_s (m/s)	P-wave amplitude (V)	S-wave amplitude (V)
0 (centered)	5839.4	2994.8	0.061	0.895
1	5783.1	3085.5	0.038	0.478
2	5930.2	3096.2	0.026	0.313
3	5825.2	2998.4	0.053	0.559
4	5911.3	3092.8	0.029	0.335
5	5925.9	3015.1	0.033	0.242
6	5869.2	3007.5	0.040	0.282
7	5911.3	2973.3	0.026	0.205
8	5827.9	3000.8	0.042	0.400

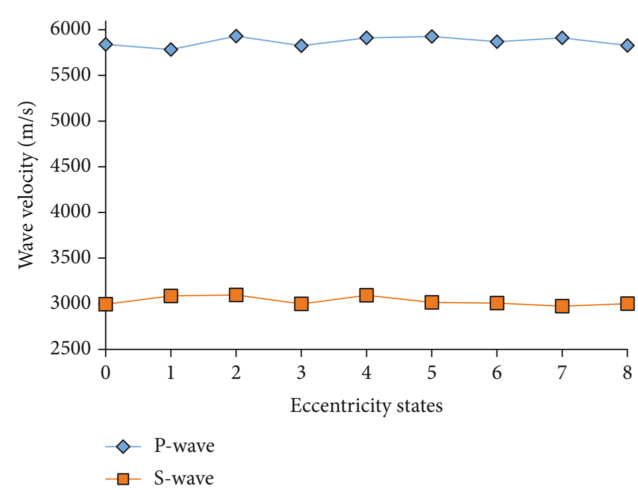

FIGURE 8: The variations of P-wave and S-wave velocities with the eccentric state when the receiver array is parallel to the borehole axis.

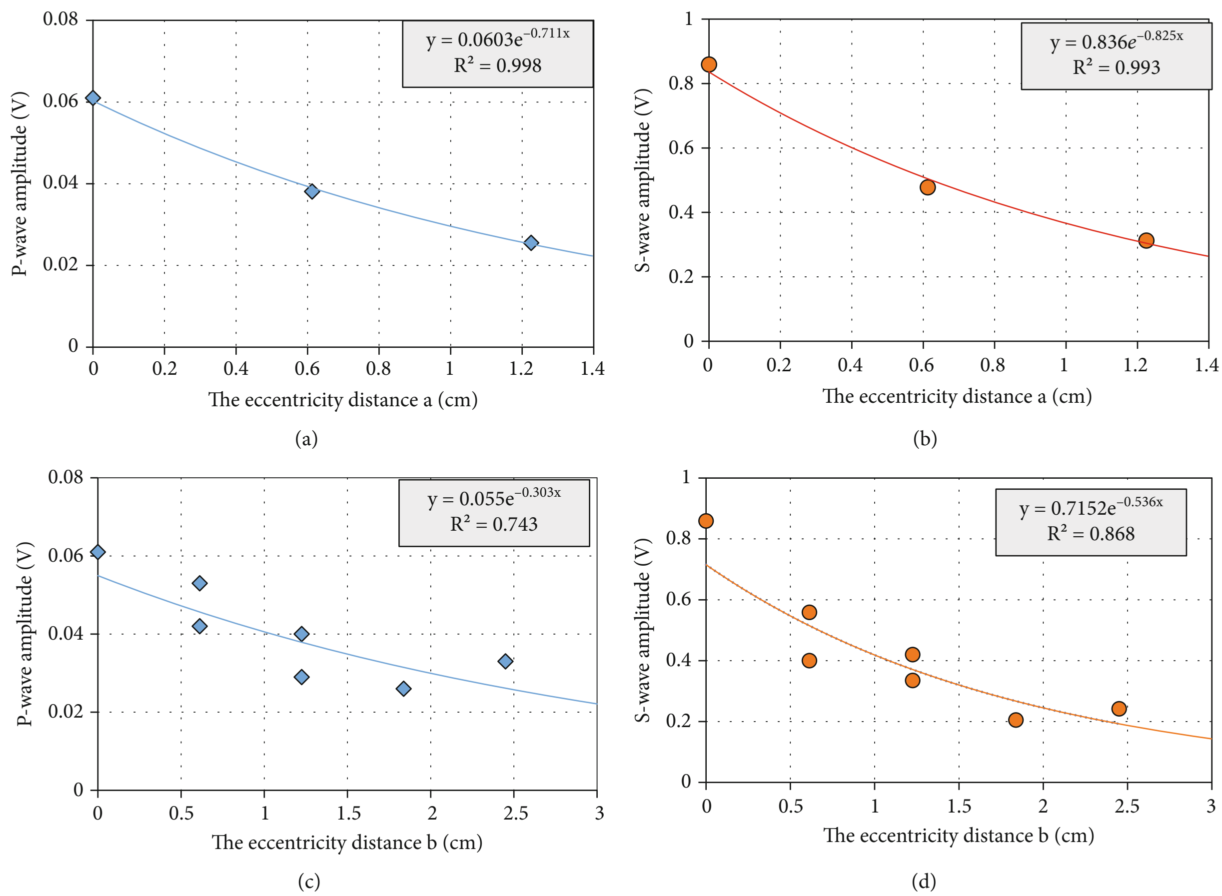

Figure 9: Variation of P-wave and S-wave amplitudes with eccentricity distances a and b when the receiver array is parallel to the borehole axis; they should be listed as (a) variation of S-wave amplitude with eccentricity distance a, (b) variation of S-wave amplitude with eccentricity distance a, (c) variation of P-wave amplitude with eccentricity distance b, and (d) variation of S-wave amplitude with eccentricity distance b.

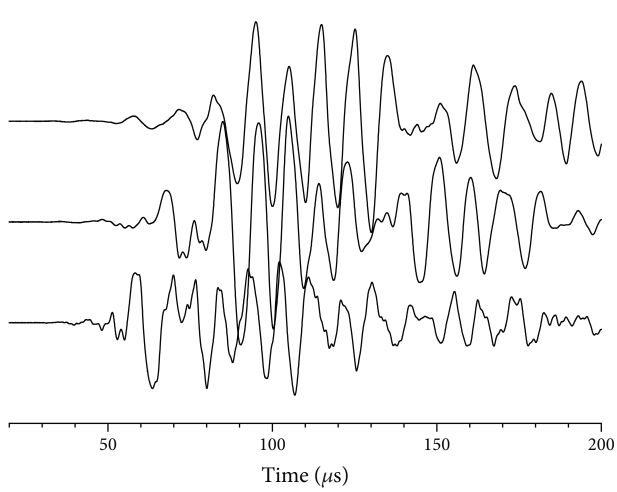

Figure 10: The array waveforms for the case the transmitter coincided with the borehole axis, and the receiver array intersected the borehole axis at 22.21°.

in Figure 12. This figure highlights that, under these conditions, both measured P-wave and S-wave velocities are significantly lower than the inherent velocities of the rocks.

Table 2: Statistical table of P-wave and S-wave velocities when the transmitter coincides with the borehole axis and the receiver array intersects the borehole axis at an angle.

Eccentricity angle (°)	0	7.75	11.54	22.21
V_p (m/s)	5839.4	10377.1	14702.7	20409.0
V_s (m/s)	2994.8	3797.5	4056.3	4230.0

Furthermore, with an increasing eccentricity angle, P-wave velocities experience a linear decline, with the rate of attenuation being markedly higher than that of S-wave velocities. Based on the preceding analysis, in this scenario, it leads to a significant increase in the time difference, resulting in a notable decrease in the calculated velocity.

4. Analysis of Influence Law of Tool Eccentricity on Array Acoustic Logging Characteristic Parameters

The experimental measurements and data analysis demonstrate that the tool eccentricity has significant impacts on the velocities and amplitudes of the waves in array acoustic

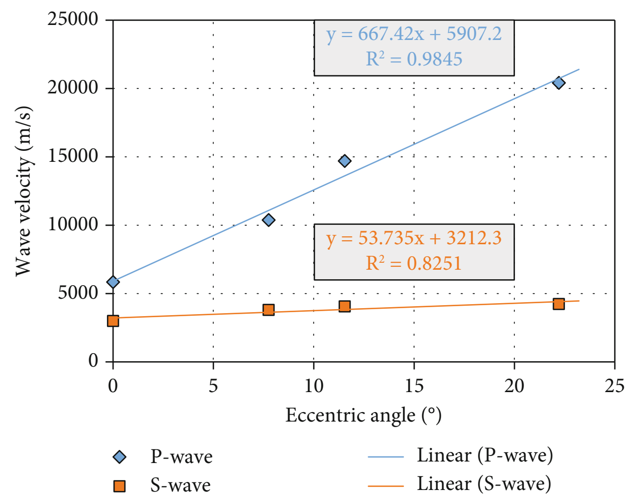

Figure 11: Relationship between P-wave and S-wave velocities with an angle when the transmitter coincides with the borehole axis and the receiver array intersects the borehole axis at an angle.

Table 3: Statistical table of P-wave and S-wave velocities when the transmitter deviates from the borehole axis and the receiver array intersects the borehole axis at an angle.

Eccentricity angle (°)	0	7.75	11.54	15.23	22.21	39.24
V_p (m/s)	5839.40	5419.33	3958.60	3797.82	3673.47	2180.23
V_s (m/s)	2994.80	2626.20	2543.64	2467.14	2450.83	1520.27

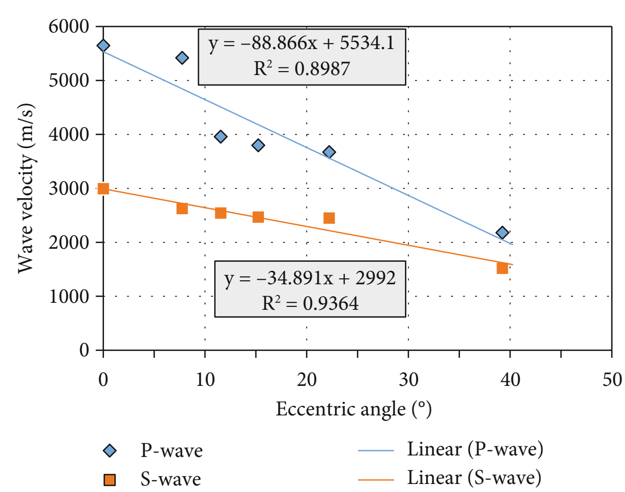

Figure 12: Relationship between P-wave and S-wave velocities with an angle when the transmitter deviates from the borehole axis and the receiver array intersects the borehole axis at an angle.

logging. Moreover, it is evident that various eccentricity states have distinct effects on wave velocities and amplitudes.

For the case where the transmitter and receiver array axes are parallel to the borehole axis, the measured P-wave velocities at different eccentricity conditions remain around 5870 m/s, with a relative error of less than 1.5%. Similarly, the S-wave velocities fluctuate around 3030 m/s, with a relative error of 2.2%. The experimental results indicate that the P-wave and S-wave velocities are not influenced by the eccentric distance in this configuration. However, when the axis of the receiver array intersects the borehole axis at an angle, the velocities of the P-wave and S-wave are significantly affected by the eccentricity angle. Modifications in the angle between the receiving array axis and the borehole axis induce variations in the mode wave velocities and, in certain scenarios, manifest as entirely antithetical patterns, as demonstrated in Figures 11 and 12. Specifically, when the transmitter axis coincides with the borehole axis and the receiver array axis intersects the borehole axis at an angle, the relationship between P-wave velocities and S-wave velocities is described by

$$\begin{cases} V_\mathrm{P} = 667.42^{*}\alpha + 5907.2\left(R^2 = 0.9845\right), \\ V_\mathrm{S} = 53.735^{*}\alpha + 3212.3\left(R^2 = 0.8251\right). \end{cases} \quad (1)$$

In formula (1), α represents the angle between the receiver array axis and the borehole axis, and the unit is degree.

Formula (2) illustrates the relationship between the P-wave velocities and the S-wave velocities when the transmitter axis deviates from the borehole axis, and the receiver array axis intersects the borehole axis at an angle.

$$\begin{cases} V_\mathrm{P} = -88.866^{*}\beta + 5534.1\left(R^2 = 0.8987\right), \\ V_\mathrm{S} = -34.891^{*}\beta + 2992\left(R^2 = 0.9364\right). \end{cases} \quad (2)$$

In formula (2), β represents the angle between the receiver array axis and the borehole axis, and the unit is degree.

Additionally, tool eccentricity can cause a notable decrease in mode wave amplitude. When the receiver array axis is parallel to the borehole axis, both P-wave and S-wave amplitudes demonstrate a negative exponential attenuation concerning the eccentricity distances "a" and "b" (Figure 9). The precise variations of P-wave and S-wave amplitudes with eccentricity distances "a" and "b" are depicted in

$$\begin{cases} A_\mathrm{P} = 0.0603e^{-0.711*\mathrm{a}}\left(R^2 = 0.998\right), \\ A_\mathrm{S} = 0.8360e^{-0.825*\mathrm{a}}\left(R^2 = 0.993\right), \end{cases} \quad (3)$$

$$\begin{cases} A_\mathrm{P} = 0.055e^{-0.303*\mathrm{b}}\left(R^2 = 0.743\right), \\ A_\mathrm{S} = 0.7152e^{-0.536*\mathrm{b}}\left(R^2 = 0.868\right). \end{cases} \quad (4)$$

In formulas (3) and (4), A_P and A_S represent the P-wave and S-wave amplitudes in V, respectively, while a and b denote the eccentric distances in centimeter.

5. Conclusions

This paper conducts a physical experiment to investigate the influence of tool eccentricity on the response of horizontal wells in array acoustic logging. Two distinct forms of eccentricity were investigated. Upon processing and analysis of the experimental data, several key conclusions were drawn:

(1) An innovative physical simulation experimental system and corresponding measurement scheme for equivalent array acoustic logging have been established and successfully deployed

(2) When the receiver array axis is parallel to the borehole axis, the velocities of the P-wave and S-wave demonstrate stability, unaffected by the eccentric distance

(3) In contrast, when the receiver array axis intersects the borehole axis at an angle, pronounced effects of tool eccentricity on the velocities of both P-wave and S-wave are observed. These velocity alterations can be attributed to the propagation paths of the wave modes, and different conditions might result in two diametrically opposed responses

(4) Additionally, tool eccentricity triggers a substantial decline in the amplitudes of the wave modes. When the receiver array axis is parallel to the borehole axis, the P-wave and S-wave amplitudes demonstrated a negative exponential relationship with the eccentricity distances "a" and "b"

These insights illuminate the intricate relationship between tool eccentricity and the responses in array acoustic logging. Additionally, the findings lay a foundation for developing appropriate data processing techniques, interpretation methods, and corrections for acoustic logging in horizontal wells. However, it is worth acknowledging a limitation of this study: its exclusive focus on the influence of tool eccentricity. As a next step, future research could broaden its scope to explore other factors that might similarly influence the responses of array acoustic logging in horizontal wells.

Data Availability

Some or all data, models, or codes generated or used during the study are available from the corresponding author by request.

Conflicts of Interest

The authors declare that there is no conflict of interest regarding the publication of this paper.

Acknowledgments

This research was funded by the National Natural Science Foundation of China (Grant Nos. 42104126 and 41774116), PetroChina Innovation Foundation (2022DQ02-0301), and Science and Technology Research Project of the Department of Education of Hubei Province, China (Grant No. Q20211309).

References

[1] X.-M. Tang, "Acoustic characterization and imaging of shale gas fractures in horizontal wells," in *Presented at the SEG International Exposition and 87th Annual Meeting*, Houston, America, 2017.

[2] C.-C. Zhou and C.-X. Wang, "Review of horizontal well logging interpretation techniques," *Advances in Geophysics*, vol. 21, no. 1, pp. 152–160, 2017.

[3] Z.-H. Wang, J.-F. Yi, and Q.-F. Zhao, "Application of geological interpretation of horizontal well logging data," *Journal of Jianghan Petroleum Institute*, vol. 3, pp. 70–78, 2004.

[4] J.-H. Wang, *Application Case Analysis of Horizontal Wells in China*, Petroleum Industry Press, Beijing, China, 2003.

[5] S.-G. Deng, *Study on Electric Logging Response of Non-uniform Formation in Highly Deviated Well, [Ph.D. thesis]*, China University of Petroleum, Qingdao City, 2006.

[6] Y.-Q. Qing, W.-R. Shi, and Y.-H. Shi, “Application test of horizontal well gas production profile logging technology in Fuling shale gas field,” *Natural Gas Exploration and Development*, vol. 39, no. 4, pp. 18–22, 2016.

[7] X. Q. Zhao, *Study on the Interpretation Method of Induction Logging for Horizontal Wells in Sand and Mudstone Section, [Ph.D. thesis]*, Jilin University, Ji Lin, 2010.

[8] Q.-Z. Cheng, X.-P. Wei, and W. Su, “Review of well logging interpretation and evaluation techniques for horizontal Wells,” *Unconventional Oil and Gas*, vol. 3, no. 2, pp. 93–98, 2016.

[9] J.-F. Guo and L. Yan, “Logging interpretation of physical parameters of horizontal well in the tight oil reservoir,” *Petroleum Geology and Engineering*, vol. 31, no. 1, pp. 76–83, 2017.

[10] J.-X. Deng and J. Yu, “Acoustic anisotropy of mudstone and shale and its influencing factors,” *Chinese Journal of Geophysics*, vol. 5, pp. 863–869, 2004.

[11] J.-Q. Zhao, C.-L. Wang, and Q.-Z. Ye, “Application of rock anisotropy in horizontal well logging interpretation,” *Well Logging Technique*, vol. 1, pp. 38–43, 1998.

[12] D. S. Fulford, “Approximation of multi-fractured horizontal well composite reservoir models using decline curves,” in *Unconventional Resources Technology Conference (URTeC)*, Austin, America, 2017.

[13] V. Dirks, X.-Q. Ma, and N. Randall, “High-resolution images from 4-C horizontal-well VSP data,” in *SEG Int'l Exposition and 72nd Annual Meeting*, Salt Lake City, America, 2002.

[14] R. Yalavarthi and R. Jayakumar, “Impact of completion design on unconventional horizontal well performance,” in *Unconventional Resources Technology Conference*, Denver, America, 2013.

[15] K. Schwartz and G. Muscio, “Petrophysical and geochemical evaluation of an Avalon shale horizontal well in the Delaware basin,” in *Unconventional resources technology conference*, Denver, America, 2014.

[16] M. Cai, H. Wu, Y. Xin et al., “Experimental study on shear wave transmission in fractured media,” *Sensors*, vol. 22, no. 11, p. 4047, 2022.

[17] M. Cai, H. Wu, P. Liu et al., “Intelligent calculation method of relative sonic attenuation and its application to fracture evaluation in tight sandstone reservoir,” *Journal of Petroleum Science and Engineering*, vol. 218, article 110968, 2022.

[18] M. Cai and C.-G. Zhang, “Experimental study on the effect of micro-fractures on shear wave attenuation and its application in fracture evaluation of tight sandstone,” *Journal of China University of Petroleum (Natural Science Edition)*, vol. 44, no. 1, pp. 45–52, 2020.

[19] S. Huang and C. Torres-Verdín, “Fast-forward modeling of compressional arrival slowness logs in high-angle and horizontal wells,” *Geophysics*, vol. 82, no. 2, pp. D107–D122, 2017.

[20] R. Wang, W. Herrera, and C. Torres-Verdín, “Simulation and interpretation of sonic waveforms in high-angle and horizontal wells,” *Geophysics*, vol. 82, no. 4, pp. D251–D263, 2017.

[21] H. Wang, G. Tao, and K. Zhang, “Wavefield simulation and analysis with the finite-element method for acoustic logging while drilling in horizontal and deviated wells,” *Geophysics*, vol. 78, no. 6, pp. D525–D543, 2013.

[22] Z.-B. Geng, *Study on Porosity Logging Correction Technology of Highly Deviated Well and Horizontal Well, [Ph.D. thesis]*, China University of Petroleum, Qingdao City, 2011.

[23] H. Liu, B. Wang, G. Tao, K. Zhang, and W. Z. Yue, “Study on the simulation of acoustic logging measurements in horizontal and deviated Wells,” *Applied Geophysics*, vol. 14, no. 3, pp. 337–350, 2017.

[24] Y. Xin, *Study on Time Difference Correction Method of Acoustic Logging in Horizontal Well and Highly Deviated Well, [M.S. thesis]*, The China University of Petroleum, Beijing, 2016.

[25] S.-L. Liu, “Analysis of the influence of foliation on logging response and rock mechanics parameters,” *Unconventional Oil and Gas*, vol. 6, no. 4, pp. 1–5, 2019.

[26] J.-S. Cong and W.-X. Qiao, “Simulation analysis of horizontal well formation interface acoustic logging response,” *Well Logging Technique*, vol. 1, pp. 29–32, 2008.

[27] H. Wang, G. Tao, and K. Zhang, “Wave field simulation and analysis with FEM for acoustic LWD in horizontal and deviated wells,” in *SEG Las Vegas 2012 Annual meeting*, Las Vegas, America, 2012.

[28] L.-S. Su, M. Cai, and Z.-S. Zheng, “Numerical simulation of the effect of borehole expansion on acoustic logging response of horizontal well,” *Geophysical and Geochemical Exploration*, vol. 46, no. 2, pp. 467–473, 2022.